Research in Pharmaceutical Sciences, October 2023; 18(5): 566-579
Received: 04-03-2023
Peer Reviewed: 10-05-2023
Revised: 27-05-2023
Accepted: 15-07-2023
Published: 20-08-2023

School of Pharmacy & Pharmaceutical Sciences
Isfahan University of Medical Sciences

Original Article

PCL/Agarose 3D-printed scaffold for tissue engineering applications: fabrication, characterization, and cellular activities

Sho'leh Ghaedamini[1], Saeed Karbasi[2], Batool Hashemibeni[1], Ali Honarvar[3], and Abbasali Rabiei[1,*]

[1]Department of Anatomical Sciences, School of Medicine, Isfahan University of Medical Sciences, Isfahan, Iran.
[2]Department of Biomaterials, Nanotechnology and Tissue Engineering, School of Advanced Technologies in Medicine, Isfahan University of Medical Sciences, Isfahan, Iran.
[3]Cellular and Molecular Research Center, Faculty of Medicine, Yasuj University of Medical Sciences, Yasuj, Iran.

Abstract

Background and purpose: Biomaterials, scaffold manufacturing, and design strategies with acceptable mechanical properties are the most critical challenges facing tissue engineering.
Experimental approach: In this study, polycaprolactone (PCL) scaffolds were fabricated through a novel three-dimensional (3D) printing method. The PCL scaffolds were then coated with 2% agarose (Ag) hydrogel. The 3D-printed PCL and PCL/Ag scaffolds were characterized for their mechanical properties, porosity, hydrophilicity, and water absorption. The construction and morphology of the printed scaffolds were evaluated *via* Fourier-Transform infrared spectroscopy (FTIR) and scanning electron microscopy (SEM). The attachment and proliferation of L929 cells cultured on the scaffolds were investigated through MTT assay on the cell culture study upon the 1st, 3rd, and 7th days.
Findings/Results: The incorporation of Ag hydrogel with PCL insignificantly decreased the mechanical strength of the scaffold. The presence of Ag enhanced the hydrophilicity and water absorption of the scaffolds, which could positively influence their cell behavior compared to the PCL scaffolds. Regarding cell morphology, the cells on the PCL scaffolds had a more rounded shape and less cell spreading, representing poor cell attachment and cell-scaffold interaction due to the hydrophobic nature of PCL. Conversely, the cells on the PCL/Ag scaffolds were elongated with a spindle-shaped morphology indicating a positive cell-scaffold interaction.
Conclusion and implications: PCL/Ag scaffolds can be considered appropriate for tissue-engineering applications.

Keywords: Agarose; Polycaprolactone; 3D printing; Tissue engineering.

INTRODUCTION

Exploring more sophisticated options to enhance the healthcare of the aged and diseased population has remained a global challenge (1, 2). Besides the increase in age-related degenerative problems and tissue loss, the growing trend in life expectancy makes it essential to use allogenic or autologous grafts for tissue-repairing targets (3). Among the several strategies toward fulfilling this goal, tissue engineering and regenerative medication (TERM) has gradually become a promising technique to satisfy the requirement of sufferers in the future. TERM aims to manufacture a three-dimensional (3D) cell/biomaterial composite, which has the same activity as a living tissue/organ and may be used to renew or regenerate a damaged tissue/organ. The essential factors in preparing such a complex are its ability to improve cell growth, nutrients and waste transportation, and gas exchange (2).

Access this article online	
	Website: http://rps.mui.ac.ir
	DOI: 10.4103/1735-5362.383711

*Corresponding author: A. Rabiei
Tel: +98-3137929026, Fax: +98-3137929105
Email: ab_rabiei@med.mui.ac.ir

Tissue engineering (TE) has been increasingly known as a valuable process for palliating the universal disease burden (4). This approach combines some factors, including cells, scaffolds, biochemical and physicochemical agents, and applies engineering technologies to modify or exchange biological tissues (5,6). Among them, scaffolds have widely attracted the attention of researchers since they can be used in the assessment, restoration or reinforcement of human tissues or organs. They provide structural support as an artificial extracellular matrix (ECM), facilitate cell proliferation, and protect their differentiation functions. Designing an ideal TE scaffold, with the ability to imitate the natural extracellular condition of the tissue, is, therefore, critical to succeed in tissue regeneration. Biocompatibility and biodegradability are other significant requirements that should be considered to promote cell adhesion. Furthermore, they should have sufficient mechanical properties to maintain 3D construction and a highly porous architecture with suitably interconnected pores to enhance cell growth and nutritious transport, thus increasing cell growth and nutrient transportation (7-9).

Salt leaching, solvent casting, gas foaming, phase separation, melt molding, and electrospinning are different methods for fabricating 3D scaffolds (9,10). However, conventional methods cannot control the pore size, porosity, geometry, and interconnectivity in the pores of the scaffolds, and fabricated scaffolds cannot be certainly modified to improve cell differentiation and tissue regeneration (11). These problems can be resolved through new 3D printing technologies based on computer-aided design and computer-aided manufacturing (12). The origin of 3D printing, referred to as additive manufacturing or rapid prototyping, dates back to the past few decades (13). A 3D printer can create a definite external and internal structure and regulate design parameters, including print speed and height of each layer (12). Fused deposition modeling (FDM) technology is a widely used 3D printing process based on extruding a molten polymer. Zhao *et al.* (14) reported that Hella cells in 3D printing models presented higher protein expression, resistance to chemotherapy, and proliferation rates when compared to the cells cultured in 2D media. In 2020, Honarvar *et al*. (15) also revealed that the presence of fibrin in polycaprolactone (PCL)/fibrin/ECM scaffolds fabricated *via* 3D printing had been improved in terms of mechanical properties, water absorption, porosity, and cell viability, as compared to particle leaching scaffolds.

Both natural and synthetic biodegradable polymers have been studied as 3D porous scaffolds for various biomedical applications. Among the synthetic polymers used in 3D printing scaffolds, PCL has been widely used for biomedical and drug delivery applications (15). Simple and easy processability, slow biodegradability, non-toxicity of its degradation products, good biocompatibility, high flexibility, strong mechanical properties, and resistance to high temperature during the melt extrusion are some advantages of this semi-crystalline linear polyester (12,15). PCL has also been approved by Food and Drug Administration (FDA) for biomedical applications. Although the absence of cell affinity in PCL because of its hydrophobicity is its drawback in TE applications (16), it can be enhanced through combining or coating with hydrophilic biopolymers such as gelatin, collagen, alginate, hyaluronic acid, and agarose (Ag) (17,18).

Ag is a natural polymer obtained from marine red algae which contains repeating units of agarobiose (a disaccharide of D-galactose and 3,6-anhydro-l-galactopyranose). Thermo-reversible gelation behavior, good biocompatibility and biodegradability, controllable oxygen and nutrient penetration, and low immune rejection potential are different features of this polymer (19,20). Ag has the same structure as ECM and high water absorbance, which can increase cell growth, differentiation, and proliferation (21). Due to the production of hydrogen bonds, cross-linking agents are not required (20). It has been demonstrated in a study that cells cultured in agarose produce more glycosaminoglycans than those cultured in other materials such as methacrylated gelatin (17).

For this research, PCL scaffolds were produced using a novel 3D printing technology; then they were coated with Ag to form PCL/Ag scaffolds. The hybrid scaffolds were studied for their *in vitro* cell culture properties, as well as their mechanical strength, morphology, hydrophilicity, and water absorption.

MATERIALS AND METHODS

PCL (80,000 g/mol) was purchased from Sigma-Aldrich (USA). Ag powder (Sinaclon, Cat. No. EP5053) was bought from Zist Exir Co. (Iran). Ultrapure water was used when preparing gels. Dulbecco's modified eagle medium-F12 (DMEM F12), phosphate-buffered saline (PBS), MTT powder (L11939 Alfa Aesar), and dimethyl sulfoxide (DMSO) were purchased from Merck (Germany). Trypsin-ethylenediaminetetraacetic acid (EDTA) and glutaraldehyde were purchased from Sigma-Aldrich (USA). Fetal bovine serum (FBS) was bought from Gibco (USA).

Preparation of PCL and PCL/Ag scaffolds

Scaffold design and 3D-printing

The 3D-printed scaffolds were designed by SOLIDWORKS® 2018 (Dassault Systèmes Solidworks Corp., Waltham, MA) software. The computer-aided design model was saved as a stereolithography (.stl) file, which allowed for direct import into the printer software. PCL granules were then melted in a heating cylinder at 80 °C, and 3D printing scaffolds were fabricated *via* Bioplotter (Envisiontec GmbH, Gladbeck, Germany). A heated nozzle extruded PCL strands onto a plate by utilizing layer-by-layer deposition (15,22). The scaffolds were prepared in conditions including 300 µm as the nozzle size, 7 mm/s as the printing speed, 700 µm as the distance between strands, and 27 G as the precision of the nozzle tip. The scaffolds were first printed in the dimensions of 20 × 20 × 4 mm^3 and then cut into a square prism shape with 5 × 5 × 4 mm^3 (23,24).

Hydrogel preparation and coating

To form a transparent hydrogel, purified Ag powder was dissolved in ultrapure water at 90 °C and then cooled up to 40 °C (25).

Coating process

Ag powder (2 g) and ultrapure water (100 mL) were mixed to make a 2 w/v% Ag solution (26,27). Ag was solubilized by boiling the solution in a microwave oven. To aid in the visualization of the composites, two drops of blue food coloring were added. The obtained solution was cooled and maintained at 45 °C using a hot-plate device (below the melting temperature of PCL and above the gelation temperature of Ag). The Ag solution (100 mL) was poured into the PCL scaffolds with the dimensions of 5 × 5 × 4 mm^3 in a vertically placed 0.5 mL EP tube. After that, the EP tube was placed under centrifugation at 4 °C to ensure a homogeneous gel distribution within the porous scaffold. Finally, after removing from the tube, the PCL/Ag scaffolds were stored at 4 °C for 30 min to allow the gelation of Ag (28).

Characterization of 3D-printed scaffolds

Morphological analysis

Scanning electron microscopy (SEM; JEOL, JSM-5200, Japan) was utilized to investigate the shape of the pores as well as their interconnectivity. The surfaces of the scaffolds were coated with gold *via* a sputter-coating machine (SC7620, Japan). The SEM images were analyzed *via* image processing software (Image J 1.51, Java 1.6.0_24 (64-bit), National Institute of Health; USA). (n = 3) (15,29).

Porosity measurements

The liquid displacement method was used to assess the porosity of the scaffold (30). Briefly, each scaffold was transported to a graduated cylinder containing a specified volume of normal hexane (V_1). The increase in hexane volume was calculated after putting the scaffold in the container (V_2). The scaffold was removed after 5 min of hexane absorption, and the container's remaining volume was estimated (V_3). The porosity percentage was calculated based on the equation (1):

$$\text{Porosity percentage } (\%) = \frac{(V1-V3)}{(V2-V3)} \times 100 \qquad (1)$$

where (V_1-V_3) is the volume of pores in the scaffold, and (V_2-V_3) is the total volume of the scaffold (n = 3) (15).

Hydrophilicity

A water contact angle test was conducted, under the standard ASTM D7334, to evaluate the scaffolds' hydrophilicity. At first, a distilled water droplet was dropped on the surface of the square prism PCL and PCL/Ag scaffolds ($5 \times 5 \times 4$ mm^3) in a horizontal plane. A photo at the 10th second was taken from the droplet by the contact angle video system (CA-ES10, Fars EOR Tech; Iran) (31). The angle between the specimen surface and the drop was measured as the contact angle *via* image processing software (Image J 1.51, Java 1.6.0_24 (64-bit), National Institute of Health; USA). The average of the right and left contact angles was calculated for each specimen (1). The data were reported as mean ± standard deviation (SD), (n = 3).

Fourier-Transform infrared spectroscopy analysis

To recognize the functional groups of pure PCL, Ag and the PCL/Ag mixture, as well as the presence of each component of materials in the scaffolds, Fourier-transform infrared spectroscopy (FTIR) was used in the attenuated total reflectance mode (FTIR-ATR, JASCO 6300; Japan). The wave number range for the spectra was 4000-400 cm^{-1}.

Water absorption capacity

Water absorption of PCL and PCL/Ag scaffolds was measured according to the ASTM-D-5964 standard. Briefly, the samples were cut into almost equal dimensions. They were first dehydrated at room temperature and then weighed; after that, each one was submerged in 10 mL of 10 mM PBS (pH 7.4). The scaffolds (n = 3) were exited from the solution after 48 h and weighed immediately after their excess water was removed (15,29). The amount of water absorption for each scaffold was calculated according to equation (2), where W_d and W_w are the weights of the specimen before and after submersion in the PBS, respectively (32).

$$Water\ absorption\ (\%) = \frac{Ww - Wd}{Ww} \times 100 \qquad (2)$$

Mechanical properties

The compressive modulus of each scaffold (5×5 mm^2) was assessed according to the ASTM E74 standard by a universal testing machine (Lloyd LRX, UK), with a load cell of 500 N, at room temperature in a dry state. The scaffolds were vertically compressed at 3 mm/min until they were reduced up to 70% of their initial thickness. The compressive modulus was calculated using the slope of the linear portion of the stress-strain curve at the 20% compressive strain (n = 3) (15,33).

Cellular evaluation

Cell preparation

L-929 mouse fibroblast cell line was obtained from Pasteur Ins. (Iran). DMEM-F12 supplemented with 10% FBS and 1% penicillin/streptomycin was consumed as the cell culturing medium. The cells were cultured in a 75 cm^2 culture flask and kept in a tissue culture incubator at 37 °C and 5% CO_2 atmosphere. Every 2 days, the culture medium was changed (30,34).

After achieving a confluence of about 90%, the cells were detached using 0.025% trypsin and 0.01% EDTA in the PBS solution; they were transferred to a centrifuge tube containing the culture medium. The cells were centrifuged, re-suspended in fresh culture media and counted before being seeded to the scaffolds (35).

In vitro cell behavior studies

The scaffolds were screened for cytotoxicity to determine their biocompatibility and potential for usage as TE scaffolds (36).

3D cell seeding

PCL and PCL/Ag scaffolds were sterilized *via* ethanol 70% overnight. They were washed three times with PBS; eventually, each side of them was exposed to UV radiation for 30 min (30,36). Before cell seeding, sterilized scaffolds were put in non-adherent cell culture microplates (Sartstedt, Nümbrecht, Germany) and submerged in the culture medium for 30 min at 37 °C to ensure cell adhesion. The corresponding cell density (2×10^4 cells) was prepared in a small-medium volume (14 µL). The cell suspension was pipetted in a drop-by-drop manner onto the center of the scaffolds. The scaffolds were incubated at 37 °C and 5% CO_2 atmosphere for 3 h to allow cell adhesion.

Next, the culture medium was perfused gently into the well along the wall until it entirely covered the scaffolds (1500 µL) (30,37). 2D cell culture in adherent cell culture microplates (Sartstedt, Germany) was employed as a control (30).

Cell morphology

After 4 days of cell culturing on the scaffolds, they were first washed twice with PBS and fixed with 4% glutaraldehyde (Merck, Germany) for 2 h. They were then gradually dehydrated with the incremental concentrations of ethanol (50, 70, 80, 90, and 100% ethanol for 30 min each). After drying, PCL and PCL/Ag scaffolds containing fixed cells were coated with gold and evaluated *via* SEM (XI30, Philips, Netherlands) (36,38).

Cell viability

The cell viability of the scaffolds was evaluated through the MTT assay. The cell-seeded scaffolds were incubated at 37 °C in 5% CO_2 and cultured for the MTT assay on the 1st, 3rd, and 7th days (15,39). The medium was replaced every 2 days (30).

In the MTT assay, the yellow tetrazolium salt was converted to violet formazan crystals through dehydrogenases produced by the mitochondria of metabolically active cells. The quantity of viable cells determines how many crystals are made from violet formazan. In this study, the culture medium was aspirated first, and scaffolds were washed with PBS twice. To analyze only the cells attached to the scaffolds, we transferred them to new wells (30,40). Next, 400 µL of the culture medium and 40 µL of the MTT solution (5 mg/mL in PBS) were added to the samples of each plate well. After that, it was incubated at 37 °C, 5% CO_2, for 4 h. After discarding the medium, 400 µL DMSO was added to each well and incubated for 2 h at room temperature. DMSO dissolves the formazan crystals and creates a purple color. Finally, 100 µL of each well was transferred to 96-well microplates, and the optical density (OD) was recorded at a wavelength of 570 nm with an ELISA microplate reader device (ZEISS, Germany). The cell viability was calculated according to equation (3), where A_s is the absorbance of cells on scaffolds, Ab_1 is the absorbance of the scaffolds without cells, A_c is the absorbance of the cells on a 24-well plate, and Ab_2 is the absorbance of the medium without cells (29,41).

$$\text{Survival rate (\%)} = \frac{As-Ab1}{Ac-Ab2} \times 100 \quad (3)$$

During each incubation period, 3 samples were evaluated, and each test was carried out in triplicate (42). The sample containing the cells plus the culturing medium without any scaffold was regarded as the cell control sample, also referred to as the tissue culture plate.

Statistical analysis

All of the quantitative data were reported as mean ± SD. One-way analysis of variance (ANOVA) followed by LSD was applied to analyze the data using statistical software (IBM, SPSS software version 11.5). *P*-values < 0.05 were considered statistically significant.

RESULTS

Morphological analysis

The SEM images of the 3D printing scaffolds displayed a macroporous arrangement along with interconnected and well-organized open pores with a uniform shape and size (Fig. 1A-C). Coating the PCL scaffolds with Ag and fabricating PCL/Ag scaffolds led to forming smooth and straight strands. Ag hydrogel successfully penetrated the scaffolds due to their open pores without filling pores (Fig. 1D-F). None of the high-magnification SEM images indicated agglomeration or clumping of the polymer or Ag.

Porosity measurements

Porosity is one of the essential parameters in selecting suitable scaffolds for cell culture and TE applications (43). In this study, porosity was higher than 80% in both groups. There was, however, no significant difference between groups regarding porosity ($P > 0.05$). The average porosity of the PCL scaffolds was 87.35%, and each pore was less than 400 µm. The PCL/Ag scaffolds had the porosity of 85.8% and a pore size of 250-400 µm (n = 3; Table 1).

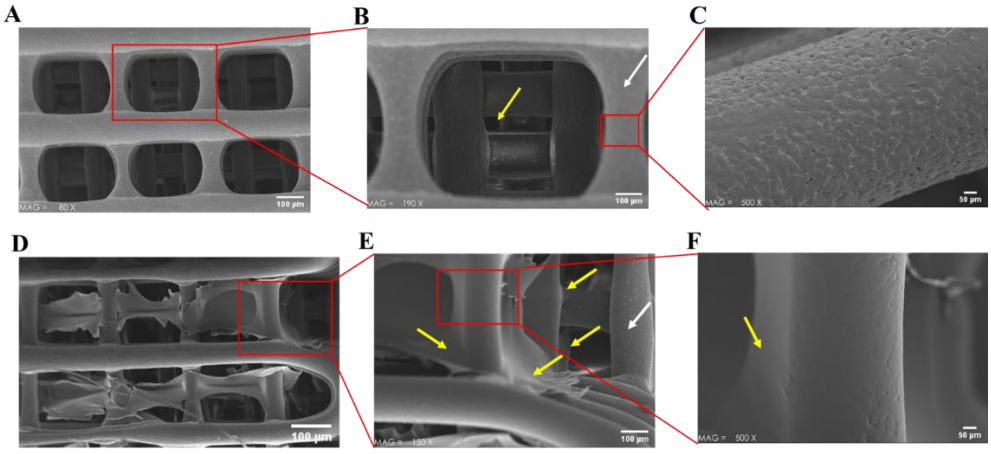

Fig. 1. Scanning electron micrographs of 3D printed scaffold. (A-C) PCL scaffold, the white arrow indicates PCL fiber, and the yellow arrow shows square interconnected pore, (D-F) PCL/Ag scaffold, yellow arrows indicate Ag coated PCL fiber (white arrow). (Scale bar 100 µm and 50 µm).

Table 1. Effects of Ag hydrogel on the compressive strength, compressive modulus, and porosity. $P > 0.05$.

Samples	Compressive strength (MPa)	Compressive modulus (MPa)	Porosity (%)
Polycaprolactone	34.76 ± 1.4	0.56 ± 0.2	87.35 ± 2.1
Polycaprolactone/agarose	29.75 ± 5.1	0.44 ± 0.2	85.8 ± 3.2

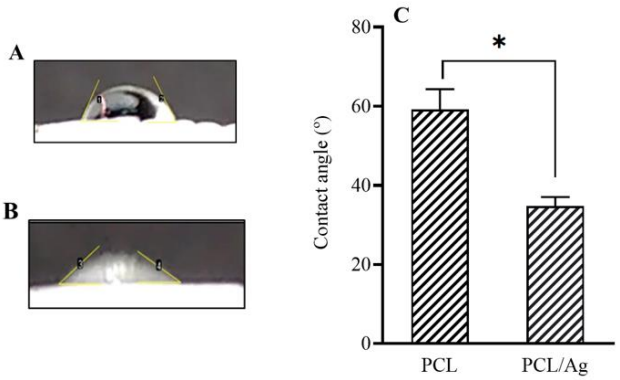

Fig. 2. Water contact angle of the scaffolds; (A) water drop on the PCL scaffold, (B) water drop on the PCL/Ag scaffold, and (C) contact angle comparison bar diagram of PCL and PCL/Ag scaffolds. *$P < 0.05$ Indicates a significant difference between the designated groups. PCL, Polycaprolactone; Ag, agarose.

Hydrophilicity

The results of the water contact angle test at the 10th second are demonstrated in Fig. 2A and B. The PCL/Ag scaffolds with a contact angle of 34.76 ± 2.35° showed more hydrophilicity, compared to the PCL scaffolds with a contact angle of 59.19 ± 5.05° (Fig. 2C). As it was expected, the high contact angle of the PCL scaffold indicated its hydrophobicity (44).

FTIR analysis

Figure 3 represents the FTIR spectra of pure components and the scaffold samples. In the Ag spectrum, the relatively weak peak at 889 cm^{-1} was related to the bending vibrations of the C-H anomeric carbon bond. The relatively weak peak at 929 cm^{-1} corresponded to the 3,6-anhydrogalactose compound (45,46). The relatively strong peaks at 1074 cm^{-1} and 1158 cm^{-1} could be attributed to the symmetric stretching vibrations of the C-O bond. The peak at 1641 cm^{-1} corresponded to the bending vibrations of the OH groups (46). The peaks that appeared at 2927 cm^{-1} and 2887 cm^{-1} could be attributed to the symmetric and asymmetric vibrations of C-H groups, respectively (45).

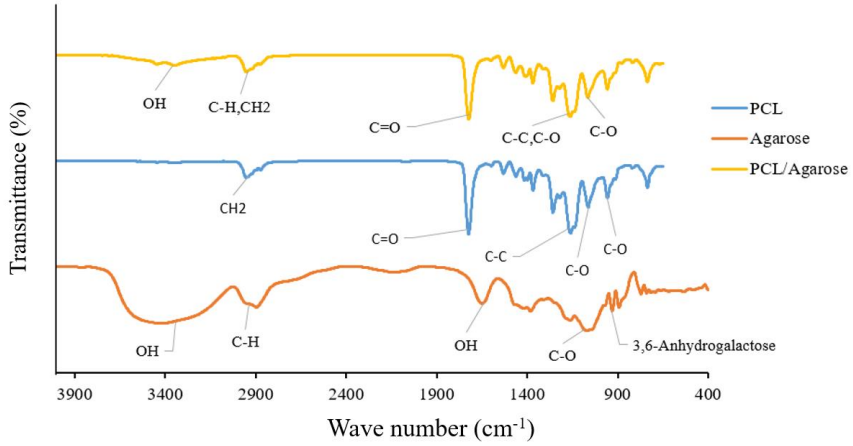

Fig. 3. Fourier-transform infrared spectroscopy spectra of pure PCL, pure Ag, and PCL/Ag scaffolds. PCL, Polycaprolactone; Ag, agarose.

On the other hand, the wide peak in the wave number range of 3062-3699 cm^{-1} was related to the symmetric stretching vibration of OH (45,46), indicating the presence of water molecules in the structure of Ag. In the PCL spectrum, the peaks in the 900-1060 cm^{-1} range were related to C-O bonds (31). The relatively strong peak at 1157 cm^{-1} could be attributed to the amorphous phase of PCL and corresponded to C-O and C-C bonds (31,47). Meanwhile, the peak at 1255 cm^{-1} corresponded to the stretching vibrations of C-O and C-C in the polymer crystal phase. The fingerprint of the ester group in PCL, as a polyester, was visible as a strong peak at 1723 cm^{-1} that was related to the carbonyl group (C=O). The relatively strong peaks at 2867 cm^{-1} and 2946 cm^{-1} corresponded to the symmetric and asymmetric stretching vibrations of CH_2, respectively (47). Observable peaks related to PCL and Ag in the PCL/Ag scaffold spectrum indicated the incorporated properties of both materials in the composite. A small increase in the intensity of the peaks at 1258 cm^{-1} (corresponding to C-O and C-C stretching vibrations in the polymer crystalline phase) and 1161 cm^{-1} (symmetric stretching vibrations of the C-O bond in Ag and amorphous PCL phase) in the PCL/Ag spectrum could indicate an increase in the number of carbon and oxygen atoms. A stronger bond between the molecules and ions in the structure followed this. The reduction in the number of free ester bonds, or, in other words, the decrease in the polarity of the bonds in the composite, led to a slight decline in the wave intensity of the ester group at 1721 cm^{-1}; this could indicate a more involvement of atoms and molecules in the composite structure than PCL and Ag alone (31). The two wide peaks at 2869 cm^{-1} and 2950 cm^{-1} corresponded to symmetric and asymmetric stretching vibrations of CH_2, respectively (47). These peaks were also visible in the pure PCL and Ag spectra. The wide peak in the range of 3148-3571 cm^{-1} in the composite spectrum was related to the symmetric stretching vibrations of hydroxyl (OH) groups due to the presence of Ag in the structure.

Water absorption capacity

The results of the water absorption test are reported in Fig. 4. It could be concluded that the combination of Ag and PCL scaffolds (PCL/Ag scaffolds) had significantly increased water uptake capacity, as compared to the PCL scaffolds. According to the obtained results, the water absorption capacity of PCL/Ag scaffolds was 59.53 ± 8.2%, and that of PCL scaffolds was 25.59 ± 9.5% (n = 3).

Mechanical properties

The 3D-printed PCL and PCL/Ag scaffolds were evaluated using the compression test. Compressive modules of the scaffolds were also calculated from the beginning gradient of the stress-strain curves (Fig. 5). Mechanical properties of the scaffolds should be in accordance with their elastic modulus and structure (48). The compressive moduli of the PCL and PCL/Ag 3D printing scaffolds were 0.56 ± 0.2 and 0.44 ± 0.2 mPa, respectively, and the compressive strength of the PCL and PCL/Ag 3D printing scaffolds was 34.76 ± 1.4 and 29.75 ± 5.1 mPa (n = 3; Table 1; $P > 0.05$), respectively.

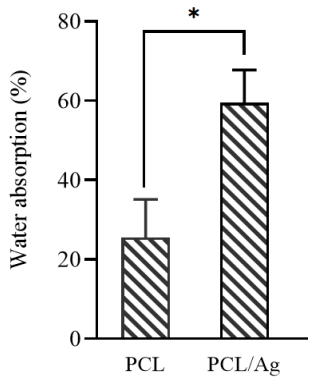

Fig. 4. Water absorption of PCL and PCL/Ag scaffolds. *P < 0.05 Indicates a significant difference between the designated groups. PCL, Polycaprolactone; Ag, agarose.

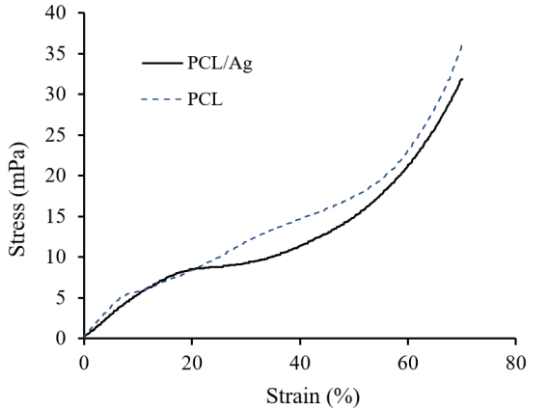

Fig. 5. Representative stress-strain curves of PCL and PCL/Ag scaffolds. PCL, Polycaprolactone; Ag, agarose.

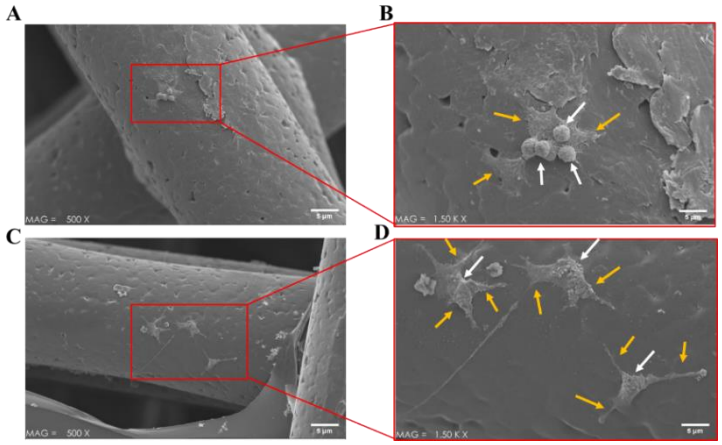

Fig. 6. Scanning electron microscopy images of L929 cells (white arrows) and pseudopodia-like extended morphology (orange arrows) on (A and B) PCL scaffold, (C and D) PCL/Ag scaffold, scale bar = 5 µm. PCL, Polycaprolactone; Ag, agarose.

Cellular evaluation

Cell morphology

Cell adhesion and morphology on the scaffolds were evaluated using SEM (49). Figure 6 shows the SEM images from the morphology of the L929 cells on the surface of PCL and PCL/Ag scaffolds. The SEM images on the 4th day after cell seeding revealed that the PCL/Ag scaffolds had a more favorable cell attachment. The morphology of the cells had a more spherical shape and less cell spreading on the PCL scaffold compared to the more stretched shape of the L929 cells on the PCL/Ag scaffold. On the other hand, the cells were significantly flattened and regularly spread with a spindle or star-like shape morphology on the PCL/Ag scaffold.

Cell viability

The scaffolds' biocompatibility and ability to support cell differentiation, adhesion, and proliferation are significant for TE applications (3,44). In this way, the cytocompatibility of the 3D printed PCL and PCL/Ag scaffolds and the impact of Ag coating were evaluated using the L929 cell line. Cell viability is a profitable procedure to evaluate the biocompatibility of the used materials for cells (50). The results of the MTT assay on the 1st, 3rd, and 7th days of cell culturing on the PCL and PCL/Ag scaffolds are demonstrated in Fig. 7. In this experiment, the cells showed the best proliferation rate at all-time points in PCL/Ag scaffolds (Fig. 7). Although PCL scaffolds presented growing cell viability and proliferation of the cell culture period, the cell viability of the PCL/Ag scaffold was significantly higher than that of other samples including tissue culture plate and the pure PCL scaffold.

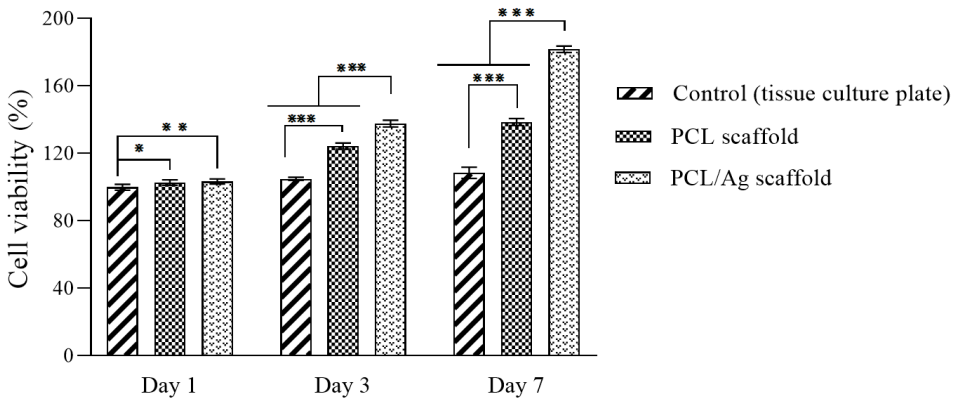

Fig. 7. Viability of L929 cells on the PCL and PCL/Ag scaffolds evaluated by MTT assay at 1st, 3rd, and 7th days; n = 6. * $P < 0.05$, ** $P < 0.01$, and *** $P < 0.001$ indicate significant differences between the designated groups

DISCUSSION

There is a growing demand for engineered human tissue equivalents for clinical and experimental purposes. TE combines cells, scaffolds, and growth factors to recover tissues or replace damaged or diseased ones (2). The 3D porous network is one of the most crucial components of the scaffold that plays a very significant role in increasing cell viability. In the FDM process, the nozzle diameter can range from 300 to 800 µm because of the viscosity of the molten polymer. Some studies suggest a thinner layer to increase surface quality and dimensional accuracy (51). Also, the printing direction and layer thickness play an essential role in the physical and mechanical properties of the scaffolds (52). In this investigation, we considered the layer thickness of 300 µm, the X direction of print, and the low temperature for the printing process. Thermo-oxidization of printing materials could be due to the high temperatures, which would cause scaffold degradation or deformation (53). PCL extrusion at 70 °C produced discontinuous and nonhomogenous strands. At the extrusion temperatures of 80 °C, 90 °C, and 100 °C, we obtained continuous and homogenous strands (54). Furthermore, Altan *et al*. (55) found that polymer could be relaxed or expanded at higher temperatures, thus implying that higher extrusion temperatures might increase dimensions. Also, the printing speed has to make a balance between the material extrusion rate and its solidification to obtain a suitable morphology. In this paper, in order to achieve excellent porosity along with appropriate morphology and mechanical strength, we chose a printing speed of 7 mm/s that improved the process efficiency by reducing the fabrication time. In another study, Soufivand *et al*. (56) concluded that decreased printing speed could reduce scaffold porosity due to the changes in filament morphological properties. Another research study also stated that elements printed with the highest printing speed had the best dimensional accuracy (57).

Cell adhesion and proliferation are greatly influenced by pore size (58). A range of 60-90% is the desired porosity in appropriate TE scaffolds. The 3D printing process is a promising method to achieve the desired porosity compared to currently available manufacturing methods (43). Pores that are too small can inhibit cell migration, while those that are too large can reduce the surface area available for cell adhesion (59). In this study, the size of pores varied from 250 to 400 µm, which could improve the cell's ability to absorb oxygen and nutrients and excrete metabolites. The results were also in agreement with another study that had reported the pore size to be from 118 to 456 µm (59). According to the FTIR results, the small change in the wave number values and also, the presence of hydroxyl peaks in the composite structure, it could be stated that some physicochemical interactions had occurred between the functional and ionic groups of Ag and PCL indicating a successful biomimetic coating for the supplemental biological investigations.

Water absorption capacity promotes the distribution of cells and the movement of

nutrients and waste in the scaffold (36). A wide range of factors, including chemical composition and permeable microstructure, could affect the scaffolds' ability to associate with water molecules (60). Hydrophilic scaffolds have been reported to enhance the cell-scaffold interactions, circulation of nutrients, secretion of ECM, and tissue growth (23,61). Our results implied that the presence of Ag increased the water absorption of the scaffolds due to their hydrophilic nature and swelling behavior. In agreement with the previous investigations, the 3D printable PCL-gelatin blends absorbed more water than the PCL scaffolds (62). 3D printed scaffolds have been reported to increase liquid exchange and absorption rates compared to fabricated scaffolds using other standard methods (15,63). Control of the design parameters and calculation of the nozzle size, porosity, interconnectivity, pore size, shape, strand distance, and orientation could be done by using the 3D printing method (24,64). In our work, Ag and 3D printing processes improved the PCL/Ag scaffold water absorption. The surface hydrophilicity of the scaffolds is an influential parameter improving protein adsorption tendency, cell attachment and proliferation. It was evaluated through the water drop contact angle test (65,66). PCL scaffolds showed an average contact angle value equal to 59.19 ± 5.05°, which was better than the previously reported values of electrospun PCL scaffolds (109° and 118°) and 3D-printed PCL scaffold (80°) (62,67,68). In addition, our work proved that combining Ag as a hydrophilic and naturally derived polymer with PCL as a synthetic polymer significantly increased the hydrophilicity of the scaffolds.

Mechanically strong biomedical scaffolds are required to successfully regenerate different tissues since the formation of new tissues and the support of their physical shape and structure highly depend on sufficient mechanical properties (69). Our results indicated that the presence of the Ag hydrogel in PCL/Ag scaffolds slightly decreased the mechanical properties of the scaffolds. In other words, the strength of the scaffolds was mostly due to PCL (70). The obtained results, thus, confirmed the investigations conducted by Dong and coworkers, which had fabricated PCL/chitosan scaffolds in a design different than ours (50). They concluded that adding chitosan hydrogel to the 3D-printed PCL scaffold did not significantly affect the PCL scaffold's mechanical properties. Buyuksungur *et al.* (70) also printed methacrylated gelatin hydrogel between the PCL fibers and found similar results, indicating that hydrogel had essentially no contribution to the mechanical properties of the PCL scaffold. In other words, the 3D printing method enables us to have a suitable macro and micro construction. Hydrogel degrades more quickly than PCL does; hence PCL will support the mechanical strength of the hybrid scaffold during tissue regeneration (70).

Biocompatibility, such as cell spreading, adhesion, proliferation, and migration on the scaffolds, is a critical perspective to assess the qualification for tissue regeneration (44). The cell morphology results were in line with the previous experiments that had refined cells on the PCL/gelatin scaffold, revealing spread shape morphologies with pseudopodia-like structures stretched to the scaffolds (71). The same type of morphology of L929 cells on the scaffold was shown in the other studies (72,73). The cells not only migrated on the surface of the scaffolds but also penetrated into interior interconnected pores. The morphology of the cells and their adhesion to the PCL/Ag scaffold confirmed that PCL and Ag had no adverse effect on the cytocompatibility of the L929 cells, thus presenting no toxicity. Unique biological properties of Ag, such as high biocompatibility and similarity to the natural ECM, can support cell attachment and growth, indicating that Ag can accelerate cell proliferation (20). These, thus, proposed the suitable biocompatibility of hybrid scaffolds compared to the hydrophobic pure PCL, due to a highly hydrated environment provided by the hybrid scaffolds. Subsequently, the hybrid scaffold indicated a biomimetic microenvironment for better cell maintenance, growth, and distribution. Ag provided a cytocompatibility environment due to its characteristic cell attachment, common swelling properties, a structure similar to that of ECM, and controllable infiltration to oxygen and nutrients, which could provide sufficient nutrient and gas exchange for the encapsulated

cells (20,74). A research study conducted by Moffat *et al*. (75) revealed that collagen content per DNA of human mesenchymal stem cells on day 28 in agarose hydrogel was higher than that of the cells in the PEG hydrogel (12). Honarvar *et al*. (15) also incorporated fibrin by adding the fibrin solution onto a 3D-printed PCL scaffold and showed that PCL/fibrin did not provide optimal conditions for cell attachment.

The PCL scaffolds printed with a suitable pore size could provide an appropriate condition for a simple penetration in the hydrogels and facilitate the transportation of oxygen and nutrients (76). Hence, the appropriated spatial pores in our constructs could also be beneficial for cell penetration and viability.

CONCLUSION

To summarize, 3D-printed scaffolds are one of the most advantageous substrates that have recently become popular in the TE field. Using the FDM technique, we fabricated a porous PCL scaffold with open and interconnected pores, as well as good mechanical properties. The arranged PCL scaffolds were coated with 2% Ag hydrogel to create the PCL/Ag scaffold in the TE field. Chemical interaction among the molecules of PCL and Ag in the PCL/Ag scaffold was shown by FTIR. Our research showed that PCL/Ag scaffolds could be more suitable for cell ingrowth than PCL ones. Ag can increase the wettability and water absorption of PCL/Ag scaffolds. High proliferation rate, admirable cell attachment, and characteristic fibroblast cell morphology over the scaffold could well indicate that the PCL/Ag scaffolds displayed in this study afforded unique openings for the TE application.

Acknowledgments

This study was financially supported by the Vice-Chancellery of Research of Isfahan University of Medical Sciences, Iran through Grant No. 3400740.

Conflict of interest statement

The authors declared no conflict of interest in this study.

Authors' contributions

S. Karbasi and Sh. Ghaedamini conceived of the presented idea; B. Hashemibeni and A. Rabiei developed the theoretical framework. S. Karbasi and A. Rabiei supervised the project; Sh. Ghaedamini and A. Honarvar carried out the experimental methods and analyzed the data; Sh. Ghaedamini and S. Karbasi equally contributed to writing the manuscript; S. Karbasi and B. Hashemibeni revised the final version of the article. All authors approved the finalized article.

REFERENCES

1. Mirmusavi MH, Ahmadian M, Karbasi S. Polycaprolactone-chitosan/multi-walled carbon nanotube: A highly strengthened electrospun nanocomposite scaffold for cartilage tissue engineering. Int J Biol Macromol. 2022;209:1801-1814. DOI: 10.1016/j.ijbiomac.2022.04.152.
2. Han F, Wang J, Ding L, Hu Y, Li W, Yuan Z, *et al*. Tissue engineering and regenerative medicine: achievements, future, and sustainability in Asia. Front Bioeng Biotechnol. 2020;8:83,1-35. DOI: 10.3389/fbioe.2020.00083.
3. O'brien FJ. Biomaterials & scaffolds for tissue engineering. Mater Today. 2011;14(3):88-95. DOI: 10.1016/S1369-7021(11)70058-X.
4. Jiang Z, He J, Wang X, Zhu D, Li N, Ren L, *et al*. Nanomaterial-based cell sheet technology for regenerative medicine and tissue engineering. Colloids Surf B Biointerfaces. 2022:112661. DOI: 10.1016/j.colsurfb.2022.112661
5. Patil S, Singh N. Antibacterial silk fibroin scaffolds with green synthesized silver nanoparticles for osteoblast proliferation and human mesenchymal stem cell differentiation. Colloids Surf B Biointerfaces. 2019;176:150-155. DOI: 10.1016/j.colsurfb.2018.12.067.
6. Hashemi-Beni B, Khoroushi M, Foroughi MR, Karbasi S, Khademi AA. Tissue engineering: dentin-pulp complex regeneration approaches (a review). Tissue Cell. 2017;49(5):552-564. DOI: 10.1016/j.tice.2017.07.002.
7. Zhou X, Zhou G, Junka R, Chang N, Anwar A, Wang H, *et al*. Fabrication of polylactic acid (PLA)-based porous scaffold through the combination of traditional bio-fabrication and 3D printing technology for bone regeneration. Colloids Surf B Biointerfaces. 2021;197:111420,1-37. DOI: 10.1016/j.colsurfb.2020.111420.
8. Kumar A, Lee Y, Kim D, Rao KM, Kim J, Park S, *et al*. Effect of crosslinking functionality on microstructure, mechanical properties, and *in vitro* cytocompatibility of cellulose nanocrystals reinforced poly (vinyl alcohol)/sodium alginate hybrid scaffolds. Int J Biol Macromol. 2017;95:962-973. DOI: 10.1016/j.ijbiomac.2016.10.085.
9. Felfel RM, Gupta D, Zabidi AZ, Prosser A, Scotchford CA, Sottile V, *et al*. Performance of multiphase scaffolds for bone repair based on two-photon polymerized poly (D,L-lactide-co-ε-

caprolactone), recombinamers hydrogel and nano-HA. Mater Des. 2018;160:455-467.
DOI: 10.1016/j.matdes.2018.09.035.
10. Movahedi M, Karbasi S. Electrospun halloysite nanotube loaded polyhydroxybutyrate-starch fibers for cartilage tissue engineering. Int J Biol Macromol. 2022;214:301-311.
DOI: 10.1016/j.ijbiomac.2022.06.072.
11. Ma H, Feng C, Chang J, Wu C. 3D-printed bioceramic scaffolds: from bone tissue engineering to tumor therapy. Acta Biomater. 2018;79:37-59.
DOI: 10.1016/j.actbio.2018.08.026.
12. Jumat MA, Chevallier P, Mantovani D, Copes F, Razak SIA, Saidin S. Three-dimensional printed biodegradable poly (L-lactic acid)/(poly (D-lactic acid) scaffold as an intervention of biomedical substitute. Polym Plast Tech Mat. 2021;60(9): 1005-1015.
DOI: 10.1080/25740881.2021.1876879.
13. Shahrubudin N, Lee TC, Ramlan R. An overview on 3D printing technology: technological, materials, and applications. Procedia Manuf. 2019;35:1286-1296.
DOI: 10.1016/j.promfg.2019.06.089.
14. Zhao Y, Yao R, Ouyang L, Ding H, Zhang T, Zhang K, *et al*. Three-dimensional printing of Hela cells for cervical tumor model *in vitro*. Biofabrication. 2014;6(3):035001,1-11.
DOI: 10.1088/1758-5082/6/3/035001.
15. Honarvar A, Karbasi S, Hashemibeni B, Setayeshmehr M, Kazemi M, Valiani A. Effects of cartilage acellular solubilised ECM on physicomechanical and biological properties of polycaprolactone/fibrin hybrid scaffold fabricated by 3D-printing and salt-leaching methods. Mater Technol. 2022;37(3):204-212.
DOI: 10.1080/10667857.2020.1824148.
16. Yang Y, Wu H, Fu Q, Xie X, Song Y, Xu M, *et al*. 3D-printed polycaprolactone-chitosan based drug delivery implants for personalized administration. Mater Des. 2022;214:110394,1-10.
DOI: 10.1016/j.matdes.2022.110394.
17. Bahcecioglu G, Hasirci N, Bilgen B, Hasirci V. Hydrogels of agarose, and methacrylated gelatin and hyaluronic acid are more supportive for *in vitro* meniscus regeneration than three dimensional printed polycaprolactone scaffolds. Int J Biol Macromol. 2019;122:1152-1162.
DOI: 10.1016/j.ijbiomac.2018.09.065.
18. Mohammadalizadeh Z, Bahremandi-Toloue E, Karbasi S. Synthetic-based blended electrospun scaffolds in tissue engineering applications. J Mater Sci. 2022;57:4020-4079.
DOI: 10.1007/s10853-021-06826-w.
19. Yazdi MK, Taghizadeh A, Taghizadeh M, Stadler FJ, Farokhi M, Mottaghitalab F, *et al*. Agarose-based biomaterials for advanced drug delivery. J Control Release. 2020;326:523-543.
DOI: 10.1016/j.jconrel.2020.07.028.
20. Zarrintaj P, Manouchehri S, Ahmadi Z, Saeb MR, Urbanska AM, Kaplan DL, *et al*. Agarose-based biomaterials for tissue engineering. Carbohydr Polym. 2018;187:66-84.
DOI: 10.1016/j.carbpol.2018.01.060.
21. Guastaferro M, Reverchon E, Baldino L. Agarose, alginate and chitosan nanostructured aerogels for pharmaceutical applications: a short review. Front Bioeng Biotechnol. 2021;9:688477,1-10.
DOI: 10.3389/fbioe.2021.688477.
22. Neufurth M, Wang X, Wang S, Steffen R, Ackermann M, Haep ND, *et al*. 3D printing of hybrid biomaterials for bone tissue engineering: calcium-polyphosphate microparticles encapsulated by polycaprolactone. Acta Biomater. 2017;64:377-388.
DOI: 10.1016/j.actbio.2017.09.031.
23. Park SA, Lee SJ, Seok JM, Lee JH, Kim WD, Kwon IK. Fabrication of 3D printed PCL/PEG polyblend scaffold using rapid prototyping system for bone tissue engineering application. J Bionic Eng. 2018;15(3):435-442.
DOI: 10.1007/s42235-018-0034-8.
24. Guo T, Lembong J, Zhang LG, Fisher JP. Three-dimensional printing articular cartilage: recapitulating the complexity of native tissue. Tissue Eng Part B Rev. 2017;23(3):225-236.
DOI: 10.1089/ten.TEB.2016.0316.
25. Arnott S, Fulmer A, Scott WE, Dea ICM, Moorhouse R, Rees DA. The agarose double helix and its function in agarose gel structure. J Mol Biol. 1974;90(2):269-84.
DOI: 10.1016/0022-2836(74)90372-6.
26. Daly AC, Critchley SE, Rencsok EM, Kelly DJ. A comparison of different bioinks for 3D bioprinting of fibrocartilage and hyaline cartilage. Biofabrication. 2016;8(4):045002,1-11.
DOI: 10.1088/1758-5090/8/4/045002.
27. Jang CH, Koo Y, Kim G. ASC/chondrocyte-laden alginate hydrogel/PCL hybrid scaffold fabricated using 3D printing for auricle regeneration. Carbohydr Polym. 2020;248:116776,1-14.
DOI: 10.1016/j.carbpol.2020.116776.
28. Aaron F, Clare M, Bastian B, Fredrick K, Tim D, Aurelien F. Dehydration-induced folding of poly (ε-caprolactone)-agarose hydrogel composites. Eur Polym J. 2019;117:159-164.
DOI: 10.1016/j.eurpolymj.2019.04.005.
29. Nikbakht M, Karbasi S, Rezayat SM. Biological evaluation of the effects of hyaluronic acid on poly (3-hydroxybutyrate) based electrospun nanocomposite scaffolds for cartilage tissue engineering application. Mater Technol. 2020;35(3):141-151.
DOI: 10.1080/10667857.2019.1659535.
30. Rabionet M, Yeste M, Puig T, Ciurana J. Electrospinning PCL scaffolds manufacture for three-dimensional breast cancer cell culture. Polymers. 2017;9(8):328,3-15.
DOI: 10.3390/polym9080328.
31. Zadehnajar P, Akbari B, Karbasi S, Mirmusavi MH. Preparation and characterization of poly ε-caprolactone-gelatin/multi-walled carbon nanotubes electrospun scaffolds for cartilage tissue engineering applications. Int J Polym Mater. 2020;69(5):326-337.
DOI: 10.1080/00914037.2018.1563088.
32. Cho YS, Hong MW, Quan M, Kim SY, Lee SH, Lee SJ, *et al*. Assessments for bone regeneration using the polycaprolactone SLUP (salt-leaching using powder)

scaffold. J Biomed Mater Res A. 2017;105(12): 3432-3444.
DOI: 10.1002/jbm.a.36196.
33. Naghieh S, Karamooz-Ravari MR, Sarker M, Karki E, Chen X. Influence of crosslinking on the mechanical behavior of 3D printed alginate scaffolds: experimental and numerical approaches. J Mech Behav Biomed Mater. 2018;80:111-118.
DOI: 10.1016/j.jmbbm.2018.01.034.
34. Kanimozhi K, Basha SK, Kumari VS, Kaviyarasu K, Maaza M. *In vitro* cytocompatibility of chitosan/PVA/ methylcellulose-nanocellulose nanocomposites scaffolds using L929 fibroblast cells. Appl Surf Sci. 2018;449:574-583.
DOI: 10.1016/j.apsusc.2017.11.197.
35. Saudi S, Bhattarai SR, Adhikari U, Khanal S, Sankar J, Aravamudhan S, *et al*. Nanonet-nano fiber electrospun mesh of PCL-chitosan for controlled and extended release of diclofenac sodium. Nanoscale. 2020;12(46):23556-23569.
DOI: 10.1039/D0NR05968D.
36. Jing X, Mi HY, Cordie T, Salick M, Peng XF, Turng LS. Fabrication of porous poly (ε-caprolactone) scaffolds containing chitosan nanofibers by combining extrusion foaming, leaching, and freeze-drying methods. Ind Eng Chem Res. 2014;53(46):17909-17918.
DOI: 10.1021/ie5034073.
37. Xue D, Zhang J, Wang Y, Mei D. Digital light processing-based 3D printing of cell-seeding hydrogel scaffolds with regionally varied stiffness. ACS Biomater Sci Eng. 2019;5(9):4825-4833.
DOI: 10.1021/acsbiomaterials.9b00696.
38. Asgarpour R, Masaeli E, Kermani S. Development of meniscus-inspired 3D-printed PCL scaffolds engineered with chitosan/extracellular matrix hydrogel. Polym Adv Technol. 2021;32(12):4721-4732.
DOI: 10.1002/pat.5465.
39. Moradi-Gharibvand N, Setayeshmehr M, Kazemi M, Safaee A, Khorsandi LS, Nejad DB, *et al*. Pomegranate seed extract enhances the inhibitory effect of adipose-derived mesenchymal stem cells on breast cancer cell line in co-culture conditions. Res Pharm Sci. 2022;17(4):372-382.
DOI: 10.4103/1735-5362.350238.
40. Teimourinejad A, Hashemibeni B, Salehi H, Mostafavi FS, Kazemi M, Bahramian H. Chondrogenic activity of two herbal products; pomegranate fruit extract and avocado/soybean unsaponifiable. Res Pharm Sci. 2020;15(4): 358-366.
DOI: 10.4103/1735-5362.293514.
41. Hashemibeni B, Valiani A, Esmaeli M, Kazemi M, Aliakbari M, Iranpour FG. Comparison of the efficacy of piascledine and transforming growth factor β1 on chondrogenic differentiation of human adipose-derived stem cells in fibrin and fibrin-alginate scaffolds. Iran J Basic Med Sci. 2018;21(2):212-218.
DOI: 10.22038/IJBMS.2018.24693.6136.
42. Kim MS, Kim G. Three-dimensional electrospun polycaprolactone (PCL)/alginate hybrid composite scaffolds. Carbohydr Polym. 2014;114:213-221.
DOI: 10.1016/j.carbpol.2014.08.008.
43. Wu Y, Sriram G, Fawzy AS, Fuh JY, Rosa V, Cao T, *et al*. Fabrication and evaluation of electrohydrodynamic jet 3D printed polycaprolactone/chitosan cell carriers using human embryonic stem cell-derived fibroblasts. J Biomater Appl. 2016;31(2):181-192.
DOI: 10.1177/088532821665253.
44. Li D, Chen W, Sun B, Li H, Wu T, Ke Q, *et al*. A comparison of nanoscale and multiscale PCL/gelatin scaffolds prepared by disc-electrospinning. Colloids Surf B Biointerfaces. 2016;146:632-641.
DOI: 10.1016/j.colsurfb.2016.07.009.
45. Sivashankari PR, Prabaharan M. Three-dimensional porous scaffolds based on agarose/chitosan/graphene oxide composite for tissue engineering. Int J Biol Macromol. 2020;146:222-231.
DOI: 10.1016/j.ijbiomac.2019.12.219.
46. Hu Z, Hong P, Liao M, Kong S, Huang N, Ou C, *et al*. Preparation and characterization of chitosan-agarose composite films. Materials. 2016;9(10):816,1-9.
DOI: 10.3390/ma9100816.
47. Elzein T, Nasser-Eddine M, Delaite C, Bistac S, Dumas P. FTIR study of polycaprolactone chain organization at interfaces. J Colloid Interface Sci. 2004;273(2):381-387.
DOI: 10.1016/j.jcis.2004.02.001.
48. Fan Z, Wang J, Liu F, Nie Y, Ren L, Liu B. A new composite scaffold of bioactive glass nanoparticles/graphene: synchronous improvements of cytocompatibility and mechanical property. Colloids Surf B Biointerfaces. 2016;145:438-446.
DOI: 10.1016/j.colsurfb.2016.05.026.
49. Mohammadalipour M, Behzad T, Karbasi S, Mohammadalipour Z. Optimization and characterization of polyhydroxybutyrate/lignin electro-spun scaffolds for tissue engineering applications. Int J Biol Macromol. 2022;218: 317-334.
DOI: 10.1016/j.ijbiomac.2022.07.139.
50. Dong L, Wang SJ, Zhao XR, Zhu YF, Yu JK. 3D-printed poly (ε-caprolactone) scaffold integrated with cell-laden chitosan hydrogels for bone tissue engineering. Sci Rep. 2017;7(1):13412,1-9.
DOI: 10.1038/s41598-017-13838-7.
51. Roberson DA, Perez ART, Shemelya CM, Rivera A, MacDonald E, Wicker RB. Comparison of stress concentrator fabrication for 3D printed polymeric izod impact test specimens. Addit Manuf. 2015;7:1-11.
DOI: 10.1016/j.addma.2015.05.002.
52. Farzadi A, Solati-Hashjin M, Asadi-Eydivand M, Abu Osman NA. Effect of layer thickness and printing orientation on mechanical properties and dimensional accuracy of 3D printed porous samples for bone tissue engineering. PloS One. 2014;9(9):e108252,1-14.
DOI: 10.1371/journal.pone.0108252.
53. Xiao X, Jiang X, Yang S, Lu Z, Niu C, Xu Y, *et al*. Solvent evaporation induced fabrication of porous polycaprolactone scaffold *via* low-temperature 3D printing for regeneration medicine researches. Polymer. 2021;217:123436,1-13.
DOI: 10.1016/j.polymer.2021.123436.
54. Sheshadri P, Shirwaiker RA. Characterization of material-process-structure interactions in the 3D

bioplotting of polycaprolactone. 3D Print Addit Manuf. 2015;2(1):20-31.
DOI: 10.1089/3dp.2014.0025.
55. Altan M, Eryildiz M, Gumus B, Kahraman Y. Effects of process parameters on the quality of PLA products fabricated by fused deposition modeling (FDM): surface roughness and tensile strength. Mater Test. 2018;60(5):471-477.
DOI: 10.3139/120.111178.
56. Soufivand AA, Abolfathi N, Hashemi A, Lee SJ. The effect of 3D printing on the morphological and mechanical properties of polycaprolactone filament and scaffold. Polym Adv Technol. 2020;31(5):1038-1046.
DOI: 10.1002/pat.4838.
57. Žarko J, Vladić G, Pál M, Dedijer S. Influence of printing speed on production of embossing tools using FDM 3D printing technology. J Graph Eng Des. 2017;8(1):19-27.
DOI: 10.24867/JGED-2017-1-019.
58. Kowalczyk P, Trzaskowska P, Łojszczyk I, Podgórski R, Ciach T. Production of 3D printed polylactide scaffolds with surface grafted hydrogel coatings. Colloids Surf B Biointerfaces. 2019;179:136-142.
DOI: 10.1016/j.colsurfb.2019.03.069.
59. Lv K, Zhu J, Zheng S, Jiao Z, Nie Y, Song F, *et al*. Evaluation of inhibitory effects of geniposide on a tumor model of human breast cancer based on 3D printed Cs/Gel hybrid scaffold. Mater Sci Eng C Mater Biol Appl. 2021;119:111509,1-10.
DOI: 10.1016/j.msec.2020.111509.
60. Pan Z, Ding J. Poly (lactide-co-glycolide) porous scaffolds for tissue engineering and regenerative medicine. Interface Focus. 2012;2(3):366-377.
DOI: 10.1098/rsfs.2011.0123.
61. Ding Y, Li W, Correia A, Yang Y, Zheng K, Liu D, *et al*. Electrospun polyhydroxybutyrate/poly (ε-caprolactone)/sol-gel-derived silica hybrid scaffolds with drug releasing function for bone tissue engineering applications. ACS Appl Mater Interfaces. 2018;10(17):14540-14548.
DOI: 10.1021/acsami.8b02656.
62. Azarudeen RS, Hassan MN, Yassin MA, Thirumarimurugan M, Muthukumarasamy N, Velauthapillai D, *et al.* 3D printable polycaprolactone-gelatin blends characterized for *in vitro* osteogenic potency. React Funct Polym. 2020;146:104445,1-24.
DOI: 10.1016/j.reactfunctpolym.2019.104445.
63. Yetiskin B, Okay O. High-strength and self-recoverable silk fibroin cryogels with anisotropic swelling and mechanical properties. Int J Biol Macromol. 2019;122:1279-1289.
DOI: 10.1016/j.ijbiomac.2018.09.087.
64. Munaz A, Vadivelu RK, John JS, Barton M, Kamble H, Nguyen N-T. Three-dimensional printing of biological matters. J Sci Adv Mater Dev. 2016;1(1):1-17.
DOI: 10.1016/j.jsamd.2016.04.001.
65. Huang A, Peng X, Geng L, Zhang L, Huang K, Chen B, *et al*. Electrospun poly (butylene succinate)/cellulose nanocrystals bio-nanocomposite scaffolds for tissue engineering: preparation, characterization and *in vitro* evaluation. Polym Test. 2018;71:101-109.
DOI: 10.1016/j.polymertesting.2018.08.027.
66. Lampin M, Warocquier-Clérout R, Legris C, Degrange M, Sigot-Luizard M. Correlation between substratum roughness and wettability, cell adhesion, and cell migration. J Biomed Mater Res. 1997;36(1):99-108.
DOI:10.1002/(SICI)1097-4636(199707)36:1<99::AID-JBM12>3.0.CO;2-E.
67. Prabhakaran MP, Venugopal JR, Chyan TT, Hai LB, Chan CK, Lim AY, *et al*. Electrospun biocomposite nanofibrous scaffolds for neural tissue engineering. Tissue Eng Part A. 2008;14(11):1787-1797.
DOI: 10.1089/ten.tea.2007.0393.
68. Zhang Y, Ouyang H, Lim CT, Ramakrishna S, Huang ZM. Electrospinning of gelatin fibers and gelatin/PCL composite fibrous scaffolds. J Biomed Mater Res Part B Appl Biomater. 2005;72(1):156-165.
DOI: 10.1002/jbm.b.30128.
69. Kim YB, Kim GH. PCL/alginate composite scaffolds for hard tissue engineering: fabrication, characterization, and cellular activities. ACS Comb Sci. 2015;17(2):87-99.
DOI: 10.1021/co500033h.
70. Buyuksungur S, Hasirci V, Hasirci N. 3D printed hybrid bone constructs of PCL and dental pulp stem cells loaded GelMA. J Biomed Mater Res A. 2021;109(12):2425-2437.
DOI: 10.1002/jbm.a.37235.
71. Cakmak AM, Unal S, Sahin A, Oktar FN, Sengor M, Ekren N, *et al*. 3D printed polycaprolactone/gelatin/bacterial cellulose/hydroxyapatite composite scaffold for bone tissue engineering. Polymers. 2020;12(9):1962,1-14.
DOI: 10.3390/polym12091962.
72. Gautam S, Chou C-F, Dinda AK, Potdar PD, Mishra NC. Fabrication and characterization of PCL/gelatin/chitosan ternary nanofibrous composite scaffold for tissue engineering applications. J Mater Sci. 2014;49(3):1076-1089.
DOI: 10.1007/s10853-013-7785-8.
73. Gautam S, Dinda AK, Mishra NC. Fabrication and characterization of PCL/gelatin composite nanofibrous scaffold for tissue engineering applications by electrospinning method. Mater Sci Eng C. 2013;33(3):1228-1235.
DOI: 10.1016/j.msec.2012.12.015.
74. Sánchez-Salcedo S, Nieto A, Vallet-Regí M. Hydroxyapatite/β-tricalcium phosphate/agarose macroporous scaffolds for bone tissue engineering. J Chem Eng. 2008;137(1):62-71.
DOI: 10.1016/j.cej.2007.09.011.
75. Moffat KL, Goon K, Moutos FT, Estes BT, Oswald SJ, Zhao X, *et al*. Composite cellularized structures created from an interpenetrating polymer network hydrogel reinforced by a 3D woven scaffold. Macromol Biosci. 2018;18(10):1800140,1-8.
DOI: 10.1002/mabi.201800140.
76. Bahcecioglu G, Hasirci N, Bilgen B, Hasirci V. A 3D printed PCL/hydrogel construct with zone-specific biochemical composition mimicking that of the meniscus. Biofabrication. 2019;11(2):025002,1-35.
DOI: 10.1088/1758-5090/aaf707.